

Gravitational waves from supercooled phase transitions and pulsar timing array signals

Jinzheng Li^a and Pran Nath^{a,*}

^a*Department of Physics, Northeastern University,
111 Forsyth Street, Boston, MA 02115-5000, U.S.A.*

E-mail: li.jinzh@northeastern.edu, p.nath@northeastern.edu

The recent detection of a gravitational wave background in the nano-Hertz frequency range by Pulsar Timing Array (PTA) collaborations, including NANOGrav, EPTA, and PPTA, has opened a new avenue for exploring fundamental physics in the early universe. In this work, we analyze a supercooled first-order phase transition in a hidden sector with a spontaneously broken $U(1)_X$ gauge symmetry as a source for this signal. We demonstrate that the thermal history of the hidden and visible sectors plays a crucial role in the gravitational wave power spectrum analysis. Our analysis shows that supercooled phase transitions can generate gravitational waves strong enough to explain the PTA observations while satisfying cosmological constraints from Big Bang Nucleosynthesis.

*Proceedings of the Corfu Summer Institute 2025 "BSM 2025 Conference" (CORFU2025) August 25–September 3, 2025
Corfu, Greece*

*Speaker

1. Introduction

The observation of gravitational waves from black hole mergers in 2016 [1] opened a new avenue to explore fundamental physics. Among various possible sources of gravitational waves, stochastic gravitational wave backgrounds are of particular interest as they could reveal fundamental new physics including inflation, cosmic strings, and cosmic phase transitions [2–4]. Recently, evidence for a signal in the Pulsar Timing Array (PTA) in the nano-Hertz frequency range ($10^{-10} - 10^{-8}$ Hz) has been found by NANOGrav [5], EPTA [6], and PPTA [7]. One of the most plausible explanations for this signal is a first-order phase transition (FOPT) during the early universe. The standard model of particle physics does not produce gravitational waves through a first-order phase transition, as the electroweak transition is a smooth crossover. This indicates that the signal must arise from physics beyond the standard model (BSM).

To reach the nano-Hertz PTA frequency range, a supercooled phase transition [8] is required for two reasons. First, a slow transition rate with small β/H is needed to generate a large enough gravitational wave power spectrum. The peak amplitude scales as

$$\Omega_{\text{GW}} h^2 \sim 10^{-6} \left(\frac{H}{\beta} \right)^2 \left(\frac{\alpha}{1 + \alpha} \right)^2, \quad (1)$$

where α is the transition strength parameter. Second, the phase transition should occur before Big Bang Nucleosynthesis (BBN) at $T \gtrsim 1$ MeV to satisfy cosmological constraints. The gravitational wave frequency in a FOPT is typically

$$f \sim 10^{-4} \frac{\beta/H}{100} \left(\frac{T}{100 \text{ GeV}} \right) \left(\frac{g_*}{100} \right)^{1/6} \text{ Hz}. \quad (2)$$

For non-supercooled transitions with large $\beta/H > 1000$, reaching nano-Hertz frequencies while maintaining $T \gtrsim 1$ MeV is not possible. This note is based on ref. [9] which examined whether supercooled FOPTs in a hidden sector can produce gravitational waves that match the PTA observations. Several challenges arise in such analyses [10]: (i) late transitions risk interfering with Big Bang Nucleosynthesis (BBN), (ii) energy release and entropy injection must not spoil light element abundances, and (iii) the transition may be too slow to complete. We demonstrate how these challenges are overcome by proper inclusion of the thermal history of the hidden and visible sectors. Similar studies on hidden sector phase transitions have been conducted in refs. [11–14].

2. A hidden sector model for gravitational wave analysis

We consider a hidden sector model coupled to the Standard Model (SM) through a kinetic mixing portal [15]. The model consists of the SM and a hidden sector charged under a $U(1)_X$ gauge symmetry with field content: A_μ (gauge field), q (Dirac fermion), Φ (complex scalar), and a kinetic energy portal. The Lagrangian is given by $\mathcal{L} = \mathcal{L}_{\text{SM}} + \Delta\mathcal{L}$ where \mathcal{L}_{SM} is the standard model Lagrangian and $\Delta\mathcal{L}$ describes the hidden sector and its coupling to the visible sector:

$$\begin{aligned} \Delta\mathcal{L} = & -\frac{1}{4} F_{\mu\nu} F^{\mu\nu} - \frac{\delta}{2} F_{\mu\nu} B^{\mu\nu} - |(\partial_\mu - ig_x A_\mu)\Phi|^2 \\ & + \bar{q}(i\gamma^\mu \partial_\mu - m_q)q - f_x \bar{q}\gamma^\mu q A_\mu - V_0^{\text{hid}}(\Phi), \end{aligned} \quad (3)$$

where A_μ is the gauge field associated with a hidden $U(1)_X$ symmetry, Φ is a complex scalar field charged under $U(1)_X$, q is a dark fermion, B_μ is the SM hypercharge gauge field, and δ is the kinetic mixing parameter. The hidden sector potential is

$$V_0^{\text{hid}} = -\mu_h^2 \Phi \Phi^* + \lambda_h (\Phi^* \Phi)^2, \quad \Phi = \frac{1}{\sqrt{2}} (\phi_c + \phi + i G_h^0), \quad (4)$$

where G_h^0 is a Goldstone boson. Thermal contributions to the zero-temperature effective potential $V_0^{\text{hid}}(\Phi)$ enable a first-order phase transition, during which the scalar field Φ acquires a vacuum expectation value (VEV). This VEV generates masses for both the hidden sector gauge boson A_μ and the scalar field ϕ itself. Three hidden sector fields A_μ, ϕ, G_h^0 contribute to the effective potential, with field-dependent masses

$$m_A^2(\phi_c) = g_x^2 \phi_c^2, \quad m_\phi^2(\phi_c) = -\mu_h^2 + 3\lambda_h \phi_c^2, \quad m_{G_h^0}^2(\phi_c) = -\mu_h^2 + \lambda_h \phi_c^2. \quad (5)$$

The effective temperature-dependent hidden sector potential including loop corrections is given by [16]

$$V_{\text{eff}}^{\text{h}}(\phi_c, T_h) = V_0^{\text{hid}}(\phi_c) + V_1^{(0)}(\phi_c) + \Delta V^{(T_h)}(\phi_c, T_h), \quad (6)$$

where $V_1^{(0)}$ is the zero-temperature one-loop Coleman-Weinberg potential and $\Delta V^{(T_h)}$ is the finite thermal correction. For $V_1^{(0)}$ we have

$$V_1^{(0)}(\phi_c) = \sum_i \frac{g_i (-1)^{2s_i}}{64\pi^2} m_i^4(\phi_c) \left[\ln \left(\frac{m_i^2(\phi_c)}{\Lambda^2} \right) - C_i \right], \quad (7)$$

where g_i is the number of degrees of freedom of particle i , s_i is its spin, and $C_i = \frac{5}{6}$ ($\frac{3}{2}$) for gauge bosons (fermions). The finite thermal correction $\Delta V^{(T_h)}$ is given by

$$\begin{aligned} \Delta V^{(T_h)}(\phi_c, T_h) &= \frac{T_h^4}{2\pi^2} \sum_{i=\text{bosons}} g_i \int_0^\infty dq \, q^2 \ln \left(1 - \exp \left(-\sqrt{q^2 + \mathcal{M}_i^2(\phi_c, T_h)/T_h^2} \right) \right) \\ &\quad - \frac{T_h^4}{2\pi^2} \sum_{i=\text{fermions}} g_i \int_0^\infty dq \, q^2 \ln \left(1 + \exp \left(-\sqrt{q^2 + \mathcal{M}_i^2(\phi_c, T_h)/T_h^2} \right) \right), \end{aligned} \quad (8)$$

where $\mathcal{M}_i^2(\phi_c, T_h)$ are thermally corrected masses using Debye masses given by

$$\begin{aligned} \mathcal{M}_i^2(\phi_c, T_h) &= m_i^2(\phi_c) + \Pi_i(T_h), \\ \Pi_A(T_h) &= \frac{2}{3} g_x^2 T_h^2, \quad \Pi_\phi(T_h) = \frac{1}{4} g_x^2 T_h^2 + \frac{1}{3} \lambda_h T_h^2. \end{aligned} \quad (9)$$

According to the model, six parameters define it: $g_x, m_q, \delta, f_x, \mu_h$ and λ_h , with an additional important parameter ξ_0 being the initial temperature ratio of the hidden and visible sectors, a topic discussed in further detail in Section 4.

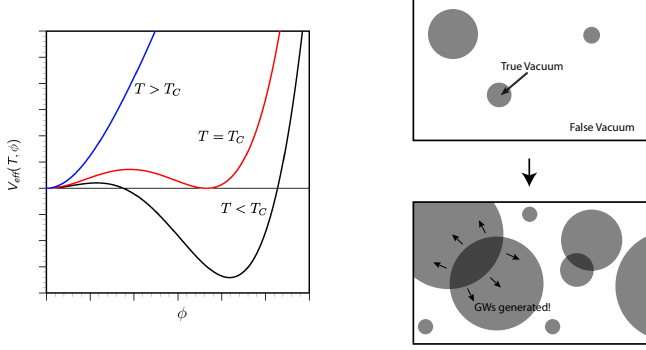


Figure 1: Illustration of the first-order phase transition showing the temperature-dependent effective potential. At the critical temperature T_c , the false and true vacua are degenerate. As the temperature decreases below T_c , the barrier between false and true vacua enables bubble nucleation and the supercooled phase transition proceeds.

3. Supercooled phase transition dynamics

A supercooled phase transition occurs when the transition temperature T_* is much lower than the critical temperature T_c , i.e., $T_*/T_c \ll 1$ [8, 17]. Such transitions are characterized by the transition temperature T_* , the transition strength α , the inverse time scale β , the bubble wall velocity v_w , and the efficiency coefficient κ [4]. The parameter space can be divided into four distinct cases based on phase transition behavior [9]:

- **Case 1:** First-order phase transitions do not occur. This includes the “ultracooled” region where the potential barrier is too large for percolation, and the “crossover” region where the transition is smooth and continuous.
- **Case 2:** Phase transitions either do not complete or the physical volume of the false vacuum does not decrease at $T_{h,p}$.
- **Case 3:** The phase transition successfully completes with a permanent potential barrier (U-shaped action curve). This case can achieve sufficiently small transition rates to fit PTA signals.
- **Case 4:** The phase transition completes with the metastable false vacuum disappearing at some non-zero temperature (“tangent-like” action curve), typically yielding larger transition rates.

The percolation temperature $T_{h,p}$ should be used to describe the transition temperature T_* for a supercooled phase transition. It is defined when 71% of the universe remains in the false vacuum [18, 19]:

$$P_f(T_{h,p}) = 0.71, \quad P_f(T_h) = \exp\left(-\frac{4\pi}{3}v_w^3 \int_{T_h}^{T_{h,c}} dT'_h \frac{\Gamma(T'_h)}{T'_h H^4(T'_h)} \left(\int_{T_h}^{T'_h} dT''_h \frac{1}{H(T''_h)}\right)^3\right), \quad (10)$$

where $\Gamma(T) \simeq T^4 \left(\frac{S(T)}{2\pi}\right)^{3/2} \exp(-S(T))$ is the bubble nucleation rate and $S(T) = S_3(T)/T$ with S_3 being the bounce action.

For supercooled phase transitions, using $\frac{\beta_*}{H_*} = T_h \left. \frac{dS(T_h)}{dT_h} \right|_{T_h=T_{h,p}}$ to characterize the transition rate leads to significant errors because it is just a linear coefficient in a Taylor expansion [4, 20]. Instead, the mean bubble separation R_* should be used, computed directly from the bubble number density [10, 21]:

$$R_*(T_h) = (n_b(T_h))^{-\frac{1}{3}} = \left(T_h^3 \int_{T_h}^{T_{h,c}} dT'_h \frac{\Gamma(T'_h) P_f(T'_h)}{T_h'^4 H(T'_h)} \right)^{-\frac{1}{3}}. \quad (11)$$

The commonly used approximation $R_* H_* \simeq (8\pi)^{1/3} v_w / (\beta/H)$ breaks down for supercooled transitions. Using β_*/H_* consistently yields larger values than $(8\pi)^{1/3} v_w / (R_* H_*)$, leading to underestimation of the final gravitational wave power spectrum. A large portion of parameter space that would be excluded by the condition $\beta_*/H_* > 3$ [22] is in fact viable when R_* is used.

4. Thermal history of hidden and visible sectors

An important element of our analysis is the synchronous evolution of the hidden and visible sectors at different temperatures [16, 23]. We define the temperature ratio $\xi(T) = T_h/T$ where T_h is the hidden sector temperature and T is the visible sector temperature. Thermal evolution of the hidden and visible sectors are affected by couplings between the two sectors, which can exist via kinetic mixing of gauge fields [15], Higgs portal couplings, or Stueckelberg mass mixing. Using energy conservation equations for the coupled sectors [24, 25]:

$$\begin{aligned} \frac{d\rho_v}{dt} + 3H(\rho_v + p_v) &= j_v, \quad (\text{visible}), \\ \frac{d\rho_h}{dt} + 3H(\rho_h + p_h) &= j_h, \quad (\text{hidden}), \end{aligned} \quad (12)$$

where j_v and j_h are interaction rates between sectors, one can derive an evolution equation for $\xi(T)$. In the limit when the couplings between the visible and the hidden sectors vanish ($j_v = j_h = 0$), the two sectors evolve independently and entropy is separately conserved in each sector, yielding [25]:

$$\xi(T)^3 \frac{h_{\text{eff}}^h(\xi(T)T)}{h_{\text{eff}}^v(T)} = \xi_0^3 \frac{h_{\text{eff}}^h(\xi_0 T_0)}{h_{\text{eff}}^v(T_0)} = \text{const}, \quad (13)$$

where $h_{\text{eff}}^{v,h}$ are the entropic effective degrees of freedom for the visible and hidden sectors, and ξ_0 is the initial temperature ratio at some reference temperature T_0 . As shown in Fig. 2, this approximation is excellent for $\delta \lesssim 10^{-10}$ but breaks down for larger kinetic mixing where energy transfer drives the sectors toward thermal equilibrium. For the benchmark points in this work with $\delta \sim 10^{-11}$, separate entropy conservation provides a reliable and computationally efficient method for tracking $\xi(T)$.

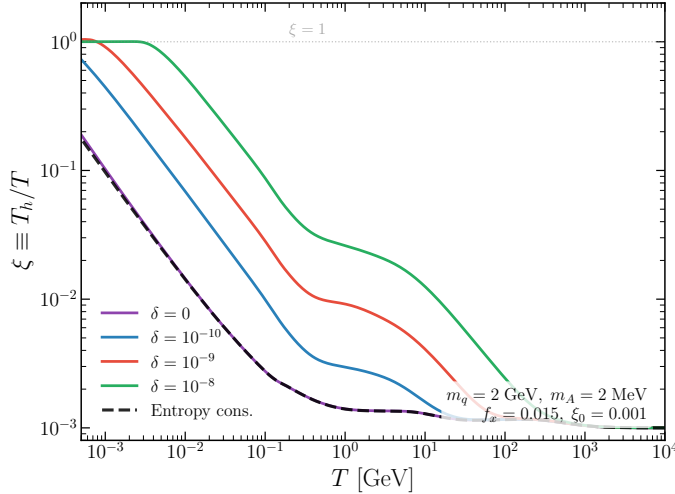


Figure 2: Evolution of the temperature ratio $\xi \equiv T_h/T$ as a function of visible sector temperature T for different values of kinetic mixing δ , with $m_q = 2$ GeV, $m_A = 2$ MeV, $f_x = 0.015$, and $\xi_0 = 0.001$. The black dashed line shows the separate entropy conservation approximation. For $\delta = 0$ and 10^{-10} , the Boltzmann solution closely follows entropy conservation. For $\delta = 10^{-9}$ and 10^{-8} , energy transfer between sectors becomes significant, driving ξ toward unity (thermalization). This demonstrates that separate entropy conservation is a good approximation only for $\delta \lesssim 10^{-10}$. Figure adapted from ref. [25].

The thermal history enters the phase transition analysis in several important ways. First, the transition strength parameters depend on the temperature ratio [14, 26]:

$$\alpha_{\text{tot}} = \frac{\Delta\bar{\theta}(T_{h,p})}{\rho_{\text{rad}}^v(T_{v,p}) + \rho_{\text{rad}}^h(T_{h,p})}, \quad \alpha_h = \frac{\Delta\bar{\theta}(T_{h,p})}{\rho_{\text{rad}}^h(T_{h,p})}, \quad (14)$$

where $\Delta\bar{\theta}$ is the vacuum energy released during the transition [27]. The parameter α_{tot} controls the gravitational wave power spectrum while α_h enters hydrodynamic calculations. For models with $g_{\text{eff}}^v \gg g_{\text{eff}}^h$, we have $\alpha_{\text{tot}} \propto \xi_p^4$, which implies that maximizing α_{tot} requires maximizing ξ_p [11]. However, the effective number of additional neutrino species scales as $\Delta N_{\text{eff}} \propto \xi_{\text{BBN}}^4$, and BBN/CMB observations impose $\Delta N_{\text{eff}} < 0.3$ [28, 29]. These conditions—maximizing α_{tot} while limiting ΔN_{eff} —are in conflict. This tension is resolved by considering a *decaying hidden sector* [14]: when hidden sector particles become non-relativistic and undergo “cannibalism” (number-changing processes like $\phi\phi\phi \rightarrow \phi\phi$) [30, 31], they consume their own particles to maintain temperature while the sector eventually decouples. This causes $g_{\text{eff}}^{h,\text{rad}}$ to decrease exponentially, driving ΔN_{eff} to zero while allowing $\xi_p \sim \mathcal{O}(1)$ during the phase transition.

Second, the Hubble parameter $H(T_h)$ depends on the total energy density including both sectors [9]:

$$H(T_h) = \sqrt{\frac{8\pi G}{3} \left(\rho_{\text{rad}}^v(T_h/\xi(T_h)) + \rho_{\text{rad}}^h(T_h) + \rho_{\text{vac}}^h(T_h) \right)}, \quad (15)$$

where ρ_{rad}^v , ρ_{rad}^h , and ρ_{vac}^h are the visible radiation, hidden radiation, and hidden vacuum energy densities, respectively. Since $H(T_h)$ appears in the percolation condition Eq. (10) and the mean bubble separation Eq. (11), a nontrivial evolution of $\xi(T_h)$ significantly affects the percolation

temperature $T_{h,p}$ and the mean bubble separation R_* . The longer integration range between $T_{h,c}$ and $T_{h,p}$ in supercooled transitions amplifies this effect.

Ignoring the ζ evolution can lead to discrepancies of up to four orders of magnitude in the predicted gravitational wave power spectrum [9]. To illustrate this, we compare two choices of $\zeta(T_h) = T_v/T_h$ in Fig. 3: a constant value $\zeta_1 = 1/\xi_p$ (the temperature ratio at percolation) and the evolving function $\zeta_2 = \zeta(T_h)$ obtained from entropy conservation. The left panel shows that the Hubble parameter $H(T_h)$ differs by a factor of $\sim 2\text{--}3$ near $T_{h,c}$, since the evolving ζ accounts for the hotter visible sector at early times (when $\xi \approx \xi_0 \ll 1$). This difference in $H(T_h)$ propagates into the percolation probability $P_f(T_h)$ (middle panel), shifting the percolation temperature by $\sim 42\%$: from $T_{h,p} = 1.11 \text{ GeV}$ with constant ζ_1 to $T_{h,p} = 0.78 \text{ GeV}$ with evolving ζ_2 . The resulting gravitational wave spectra (right panel) differ by over an order of magnitude in amplitude and exhibit a frequency shift, with only the evolving case reaching the PTA-sensitive nano-Hertz region. This demonstrates the necessity of self-consistently tracking the thermal evolution of both sectors.

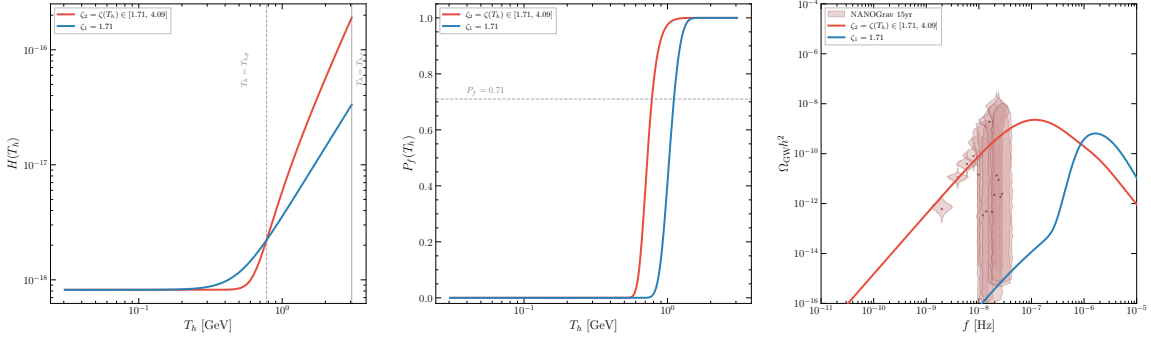


Figure 3: Comparison of a constant vs an evolving temperature ratio $\zeta(T_h) = T_v/T_h$ for BP1. Left: Hubble parameter $H(T_h)$ as a function of hidden sector temperature. The dashed vertical line marks the percolation temperature $T_{h,p}$ and the solid line marks the critical temperature $T_{h,c}$. Middle: False vacuum survival probability $P_f(T_h)$; the horizontal dashed line marks $P_f = 0.71$. Right: Gravitational wave power spectrum with NANOGrav 15yr data. The red curves use the evolving $\zeta_2 = \zeta(T_h) \in [1.71, 4.09]$ from entropy conservation, while the blue curves use a constant $\zeta_1 = 1/\xi_p = 1.71$. Figure adapted from ref. [9].

5. Gravitational wave power spectrum

The gravitational wave power spectrum receives contributions from three sources: bubble collisions, sound waves in the plasma, and turbulence in the plasma [2, 3, 32]:

$$\Omega_{\text{GW}} \simeq \Omega_{\text{col}} + \Omega_{\text{sw}} + \Omega_{\text{turb}}. \quad (16)$$

The relative importance of these contributions depends on whether the bubble expansion is in the runaway or non-runaway regime. If a true vacuum bubble generated during the phase transition continues to accelerate to a velocity close to the speed of light ($v_w \simeq 1$), this is referred to as the runaway scenario, and most of the energy is stored in the bubble walls so that gravitational waves are predominantly generated by bubble collisions. Conversely, if the bubble reaches a terminal velocity $v_w < 1$ (non-runaway scenario), most of the energy resides in the plasma and gravitational waves are primarily produced by sound waves and turbulence. The classification is made using a

critical phase transition strength [2, 33]:

$$\alpha_{h,\infty} = \frac{T_{h,p}^2}{\rho_{\text{rad}}^h(T_{h,p})} \left(\sum_{i=\text{bosons}} n_i \frac{\Delta m_i^2}{24} + \sum_{i=\text{fermions}} n_i \frac{\Delta m_i^2}{48} \right). \quad (17)$$

When $\alpha_h > \alpha_{h,\infty}$, the scenario is runaway, and the efficiency factors are given by $\kappa_\phi = 1 - \alpha_{h,\infty}/\alpha_h$ and $\kappa_{\text{sw}} = (\alpha_{h,\infty}/\alpha_h)\kappa(\alpha_{h,\infty}, c_{s,f}^2, c_{s,t}^2, v_w)$, where κ is the transition coefficient calculated using the method of refs. [26, 27]. The kinetic energy fraction is then

$$K = \frac{\alpha_{\text{tot}}}{1 + \alpha_{\text{tot}}} \kappa(c_{s,f}^2, c_{s,t}^2, \alpha_h, v_w). \quad (18)$$

Our analysis shows that for supercooled phase transitions capable of producing a PTA signal, α_h is generally too large to yield deflagration or hybrid solutions, and all PTA events are of the detonation type with bubble wall velocity approximated by the Chapman-Jouguet velocity [34, 35]:

$$v_w \approx v_J = c_{s,f} \left(\frac{1 + \sqrt{3\alpha_h(1 + c_{s,f}^2(3\alpha_h - 1))}}{1 + 3\alpha_h c_{s,f}^2} \right). \quad (19)$$

In the envelope approximation [36, 37], the bubble collision contribution is

$$h^2 \Omega_{\text{col}}(f) = 1.67 \times 10^{-5} \left(\frac{H_*}{\beta} \right)^2 \left(\frac{\kappa_\phi \alpha}{1 + \alpha} \right)^2 \left(\frac{100}{g_*} \right)^{1/3} \frac{0.11 v_w^3}{0.42 + v_w^2} S_{\text{col}}(f), \quad (20)$$

with spectral shape $S_{\text{col}}(f) = 3.8(f/f_{\text{col}})^{2.8}/[1 + 2.8(f/f_{\text{col}})^{3.8}]$. We provide five benchmark points in Table 1 that generate sufficiently strong gravitational waves to match the PTA signal while satisfying cosmological constraints. The resulting phase transition parameters are listed in Table 2.

	m_q	g_x	f_x	$\delta(\times 10^{-12})$	ξ_0	μ_h	λ_h	m_A	m_ϕ
(BP1)	16.25	2.500	0.066	15.0	0.190	3.150	0.490	11.25	4.45
(BP2)	24.50	2.700	0.100	5.0	0.210	5.652	0.652	18.90	7.99
(BP3)	28.00	2.200	0.075	30.0	0.160	4.433	0.307	17.60	6.27
(BP4)	56.00	2.000	0.114	8.0	0.220	7.470	0.218	32.00	10.57
(BP5)	14.13	2.500	0.058	20.0	0.180	2.555	0.490	9.13	3.61

Table 1: Benchmark points BP1-BP5 for the model parameters. All masses are in units of GeV. The scalar-gauge coupling g_x determines the Coleman-Weinberg potential and the phase transition dynamics, while the fermion-gauge coupling f_x controls the dark matter annihilation cross-section and relic density. The values of f_x are chosen to yield $\Omega_{DM} h^2$ close to the observed value.

	$T_{h,p}$	$T_{h,reh}$	$T_{h,c}$	$T_{v,p}$	ξ_p	α_{tot}	α_h	$\frac{\beta_*}{H_*}$	$\frac{(8\pi)^{1/3}v_w}{H_*R_*}$	$\Omega_{DM}h^2$
(BP1)	0.778	2.021	3.053	1.330	0.585	0.284	305	-227.34	4.38	0.114
(BP2)	1.318	3.337	5.093	1.857	0.709	0.534	337	-224.38	4.20	0.113
(BP3)	0.906	3.231	4.865	1.387	0.653	1.964	2766	-316.70	3.59	0.111
(BP4)	1.959	6.009	9.008	3.023	0.648	0.852	549	-255.54	3.42	0.110
(BP5)	0.658	1.645	2.476	1.254	0.525	0.153	222	-215.79	4.14	0.112

Table 2: Output parameters for benchmarks BP1-BP5. $T_{h,p}$ and $T_{v,p}$ are the percolation temperatures for the hidden and visible sectors, $T_{h,reh}$ and $T_{h,c}$ are the reheat and critical temperatures, and ξ_p is the temperature ratio at percolation. All temperatures are in GeV. Note that β_*/H_* is negative, which would exclude these points under the traditional constraint $\beta_*/H_* > 3$, but they are valid using R_* . All benchmarks belong to Case 3. The fermion-gauge coupling f_x is tuned to yield $\Omega_{DM}h^2$ consistent with the observed value $\Omega_{DM}h^2 \simeq 0.12$ [28].

In Table 2, we observe that the temperature ratio during the phase transition, ξ_p , ranges from 0.53 to 0.71, enabling strong phase transitions with α_{tot} ranging from 0.15 to 1.96. For all benchmark points, the hidden sector becomes non-relativistic before BBN, satisfying ΔN_{eff} constraints. Our calculations show that β_*/H_* is negative for these benchmark points; while this would have excluded them under the constraint $\beta_*/H_* > 3$, these points are valid since we employ the mean bubble separation R_* instead. For all benchmarks, we find $\alpha_{h,\infty} < \alpha_h$, confirming they are in the runaway regime. The calculated gravitational wave power spectra for all benchmark points are displayed in Fig. 4. These spectra reach and in some cases exceed the observed PTA signal. The right panel illustrates the detection regions of future space-based gravitational wave detectors, showing that the power spectra from our benchmark points fall within these detection regions, providing further tests of the supercooled phase transition scenario.

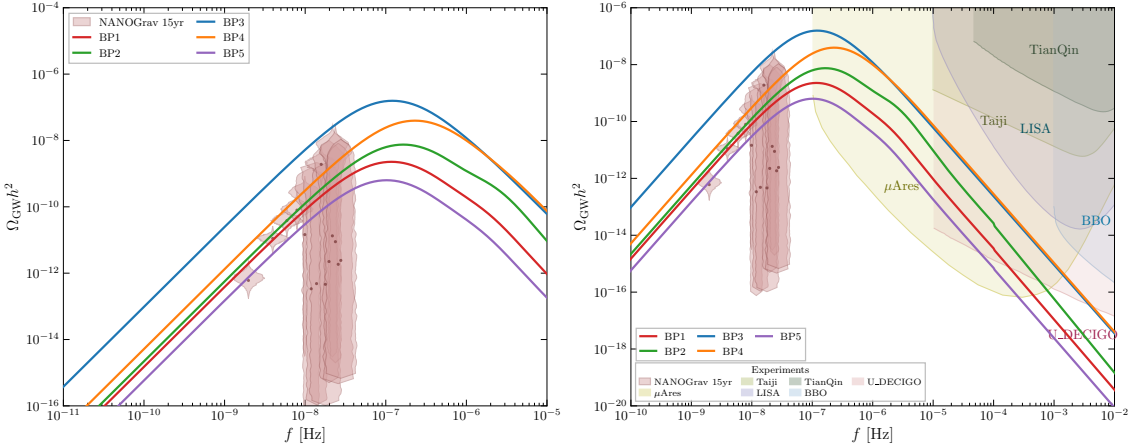


Figure 4: Left panel: The gravitational wave power spectrum $\Omega_{\text{GW}}h^2$ for supercooled phase transitions as a function of frequency for five benchmark points BP1–BP5 in the range $[10^{-11}–10^{-5}]$ Hz. The shaded violins represent the NANOGrav 15yr free-spectrum posterior [5]. Right panel: Projected sensitivity regions of future space-based GW detectors including μAres [38], Taiji [39], LISA [40], TianQin [41], BBO [42], and U-DECIGO [43]. The benchmark spectra fall within multiple detector sensitivity regions, providing further tests of the supercooled phase transition scenario. Figure adapted from ref. [9].

As shown in Fig. 5, for supercooled phase transitions generating PTA signals, bubble collisions

make the dominant contribution in the nano-Hertz region, while sound waves and turbulence are highly suppressed.

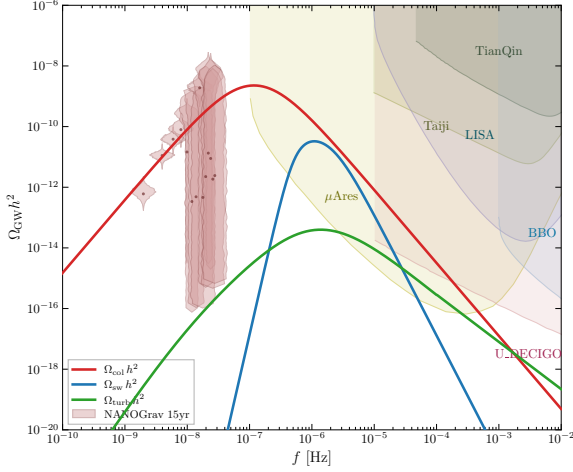


Figure 5: The three primary contributions to the gravitational wave signal for BP1: bubble collisions (red), sound waves (blue), and turbulence (green). The bubble collision contribution dominates by several orders of magnitude in the nano-Hz PTA region, while sound waves and turbulence are negligible. The shaded regions indicate projected sensitivities of future space-based detectors. Figure adapted from ref. [9].

6. Conclusion

We have demonstrated that the thermal history of the hidden sector enters crucially in the analysis of pulsar timing array signals. Taking the thermal history of the hidden versus visible sectors into account, first-order supercooled phase transitions can generate stochastic gravitational waves that explain the observations of NANOGrav, EPTA, and PPTA. Our analysis emphasizes several key aspects: (i) the use of mean bubble separation R_* rather than the inverse timescale β_* for characterizing supercooled phase transitions—a large portion of parameter space excluded by $\beta_*/H_* > 3$ is viable when R_* is used; (ii) the importance of synchronous evolution of hidden and visible sector temperatures; (iii) the resolution of the tension between maximizing α_{tot} for PTA signals and satisfying ΔN_{eff} constraints through a decaying hidden sector undergoing cannibalism. The benchmark models presented here not only match current PTA observations but also predict signals within the detection range of future space-based gravitational wave detectors such as LISA, Taiji, TianQin, and DECIGO, providing further tests of supercooled phase transition scenarios.

Acknowledgments

The research of PN was supported in part by the NSF Grant PHY-2209903.

References

[1] B. P. Abbott *et al.* [LIGO Scientific and Virgo], Phys. Rev. Lett. **116**, no.6, 061102 (2016) doi:10.1103/PhysRevLett.116.061102 [arXiv:1602.03837 [gr-qc]].

[2] C. Caprini, M. Hindmarsh, S. Huber, T. Konstandin, J. Kozaczuk, G. Nardini, J. M. No, A. Petiteau, P. Schwaller and G. Servant, *et al.* JCAP **04**, 001 (2016) doi:10.1088/1475-7516/2016/04/001 [arXiv:1512.06239 [astro-ph.CO]].

[3] C. Caprini, M. Chala, G. C. Dorsch, M. Hindmarsh, S. J. Huber, T. Konstandin, J. Kozaczuk, G. Nardini, J. M. No and K. Rummukainen, *et al.* JCAP **03**, 024 (2020) doi:10.1088/1475-7516/2020/03/024 [arXiv:1910.13125 [astro-ph.CO]].

[4] P. Athron, C. Balázs, A. Fowlie, L. Morris and L. Wu, Prog. Part. Nucl. Phys. **135**, 104094 (2024) doi:10.1016/j.ppnp.2023.104094 [arXiv:2305.02357 [hep-ph]].

[5] G. Agazie *et al.* [NANOGrav], Astrophys. J. Lett. **951**, no.1, L8 (2023) doi:10.3847/2041-8213/acdac6 [arXiv:2306.16213 [astro-ph.HE]].

[6] J. Antoniadis *et al.* [EPTA and InPTA:], Astron. Astrophys. **678**, A50 (2023) doi:10.1051/0004-6361/202346844 [arXiv:2306.16214 [astro-ph.HE]].

[7] D. J. Reardon, A. Zic, R. M. Shannon, G. B. Hobbs, M. Bailes, V. Di Marco, A. Kapur, A. F. Rogers, E. Thrane and J. Askew, *et al.* Astrophys. J. Lett. **951**, no.1, L6 (2023) doi:10.3847/2041-8213/acdd02 [arXiv:2306.16215 [astro-ph.HE]].

[8] S. W. Hawking and I. G. Moss, Phys. Lett. B **110**, 35-38 (1982) doi:10.1016/0370-2693(82)90946-7

[9] J. Li and P. Nath, Phys. Rev. D **111**, no.12, 123007 (2025) doi:10.1103/79cb-rssl [arXiv:2501.14986 [hep-ph]].

[10] P. Athron, A. Fowlie, C. T. Lu, L. Morris, L. Wu, Y. Wu and Z. Xu, Phys. Rev. Lett. **132**, no.22, 221001 (2024) doi:10.1103/PhysRevLett.132.221001 [arXiv:2306.17239 [hep-ph]].

[11] M. Breitbach, J. Kopp, E. Madge, T. Opferkuch and P. Schwaller, JCAP **07**, 007 (2019) doi:10.1088/1475-7516/2019/07/007 [arXiv:1811.11175 [hep-ph]].

[12] P. Schwaller, Phys. Rev. Lett. **115**, no.18, 181101 (2015) doi:10.1103/PhysRevLett.115.181101 [arXiv:1504.07263 [hep-ph]].

[13] M. Fairbairn, E. Hardy and A. Wickens, JHEP **07**, 044 (2019) doi:10.1007/JHEP07(2019)044 [arXiv:1901.11038 [hep-ph]].

[14] T. Bringmann, P. F. Depta, T. Konstandin, K. Schmidt-Hoberg and C. Tasillo, JCAP **11**, 053 (2023) doi:10.1088/1475-7516/2023/11/053 [arXiv:2306.09411 [astro-ph.CO]].

[15] B. Holdom, Phys. Lett. B **166**, 196-198 (1986) doi:10.1016/0370-2693(86)91377-8

[16] W. Z. Feng, J. Li and P. Nath, Phys. Rev. D **110**, no.1, 015020 (2024) doi:10.1103/PhysRevD.110.015020 [arXiv:2403.09558 [hep-ph]].

[17] J. Ellis, M. Lewicki and J. M. No, JCAP **04**, 003 (2019) doi:10.1088/1475-7516/2019/04/003 [arXiv:1809.08242 [hep-ph]].

[18] P. Athron, C. Balázs and L. Morris, *JCAP* **03**, 006 (2023) doi:10.1088/1475-7516/2023/03/006 [arXiv:2212.07559 [hep-ph]].

[19] X. Wang, F. P. Huang and X. Zhang, *JCAP* **05**, 045 (2020) doi:10.1088/1475-7516/2020/05/045 [arXiv:2003.08892 [hep-ph]].

[20] A. Megevand and S. Ramirez, *Nucl. Phys. B* **919**, 74-109 (2017) doi:10.1016/j.nuclphysb.2017.03.009 [arXiv:1611.05853 [astro-ph.CO]].

[21] K. Enqvist, J. Ignatius, K. Kajantie and K. Rummukainen, *Phys. Rev. D* **45**, 3415-3428 (1992) doi:10.1103/PhysRevD.45.3415

[22] M. S. Turner, E. J. Weinberg and L. M. Widrow, *Phys. Rev. D* **46**, 2384-2403 (1992) doi:10.1103/PhysRevD.46.2384

[23] A. Aboubrahim and P. Nath, *JHEP* **09**, 084 (2022) doi:10.1007/JHEP09(2022)084 [arXiv:2205.07316 [hep-ph]].

[24] A. Aboubrahim, W. Z. Feng, P. Nath and Z. Y. Wang, *Phys. Rev. D* **103**, no.7, 075014 (2021) doi:10.1103/PhysRevD.103.075014 [arXiv:2008.00529 [hep-ph]].

[25] J. Li and P. Nath, *Phys. Rev. D* **108**, no.11, 115008 (2023) doi:10.1103/PhysRevD.108.115008 [arXiv:2304.08454 [hep-ph]].

[26] F. Giese, T. Konstandin, K. Schmitz and J. van de Vis, *JCAP* **01**, 072 (2021) doi:10.1088/1475-7516/2021/01/072 [arXiv:2010.09744 [astro-ph.CO]].

[27] F. Giese, T. Konstandin and J. van de Vis, *JCAP* **07**, no.07, 057 (2020) doi:10.1088/1475-7516/2020/07/057 [arXiv:2004.06995 [astro-ph.CO]].

[28] N. Aghanim *et al.* [Planck], *Astron. Astrophys.* **641**, A6 (2020) [erratum: *Astron. Astrophys.* **652**, C4 (2021)] doi:10.1051/0004-6361/201833910 [arXiv:1807.06209 [astro-ph.CO]].

[29] R. H. Cyburt, B. D. Fields, K. A. Olive and T. H. Yeh, *Rev. Mod. Phys.* **88**, 015004 (2016) doi:10.1103/RevModPhys.88.015004 [arXiv:1505.01076 [astro-ph.CO]].

[30] M. Farina, D. Pappadopulo, J. T. Ruderman and G. Trevisan, *JHEP* **12**, 039 (2016) doi:10.1007/JHEP12(2016)039 [arXiv:1607.03108 [hep-ph]].

[31] F. Ertas, F. Kahlhoefer and C. Tasillo, *JCAP* **02**, no.02, 014 (2022) doi:10.1088/1475-7516/2022/02/014 [arXiv:2109.06208 [astro-ph.CO]].

[32] D. J. Weir, *Phil. Trans. Roy. Soc. Lond. A* **376**, no.2114, 20170126 (2018) [erratum: *Phil. Trans. Roy. Soc. Lond. A* **381**, 20230212 (2023)] doi:10.1098/rsta.2017.0126 [arXiv:1705.01783 [hep-ph]].

[33] D. Bodeker and G. D. Moore, *JCAP* **05**, 025 (2017) doi:10.1088/1475-7516/2017/05/025 [arXiv:1703.08215 [hep-ph]].

[34] J. R. Espinosa, T. Konstandin, J. M. No and G. Servant, JCAP **06**, 028 (2010) doi:10.1088/1475-7516/2010/06/028 [arXiv:1004.4187 [hep-ph]].

[35] W. Y. Ai, B. Laurent and J. van de Vis, JCAP **07**, 002 (2023) doi:10.1088/1475-7516/2023/07/002 [arXiv:2303.10171 [astro-ph.CO]].

[36] S. J. Huber and T. Konstandin, JCAP **09**, 022 (2008) doi:10.1088/1475-7516/2008/09/022 [arXiv:0806.1828 [hep-ph]].

[37] A. Kosowsky and M. S. Turner, Phys. Rev. D **47**, 4372-4391 (1993) doi:10.1103/PhysRevD.47.4372 [arXiv:astro-ph/9211004 [astro-ph]].

[38] A. Sesana, N. Korsakova, M. A. Sedda, V. Baibhav, E. Barausse, S. Barke, E. Berti, M. Bonetti, P. R. Capelo and C. Caprini, *et al.* Exper. Astron. **51**, no.3, 1333-1383 (2021) doi:10.1007/s10686-021-09709-9 [arXiv:1908.11391 [astro-ph.IM]].

[39] W. H. Ruan, Z. K. Guo, R. G. Cai and Y. Z. Zhang, Int. J. Mod. Phys. A **35**, no.17, 2050075 (2020) doi:10.1142/S0217751X2050075X [arXiv:1807.09495 [gr-qc]].

[40] P. Amaro-Seoane *et al.* [LISA], [arXiv:1702.00786 [astro-ph.IM]].

[41] J. Luo *et al.* [TianQin], Class. Quant. Grav. **33**, no.3, 035010 (2016) doi:10.1088/0264-9381/33/3/035010 [arXiv:1512.02076 [astro-ph.IM]].

[42] C. Grojean and G. Servant, Phys. Rev. D **75**, 043507 (2007) doi:10.1103/PhysRevD.75.043507 [arXiv:hep-ph/0607107 [hep-ph]].

[43] S. Kawamura, T. Nakamura, M. Ando, N. Seto, K. Tsubono, K. Numata, R. Takahashi, S. Nagano, T. Ishikawa and M. Musha, *et al.* Class. Quant. Grav. **23**, S125-S132 (2006) doi:10.1088/0264-9381/23/8/S17